DR. JIA GUO (Orcid ID : 0000-0003-3371-5857)

Article type : Full Paper

Comparison of velocity selective arterial spin labeling schemes

Jia Guo [1*], Shaurov Das [1], Luis Hernandez-Garcia [2,3]

1. Department of Bioengineering, University of California Riverside, Riverside, CA, USA;
2. Department of Biomedical Engineering, University of Michigan, Ann Arbor, MI, USA
3. FMRI Laboratory, University of Michigan, Ann Arbor, MI, USA

* **Correspondence**

Jia Guo

Department of Bioengineering

900 University Ave, MS&E 205

University of California Riverside

Riverside, CA 92521, USA

Email: jia.guo@ucr.edu

This is the author manuscript accepted for publication and has undergone full peer review but has not been through the copyediting, typesetting, pagination and proofreading process, which may lead to differences between this version and the Version of Record. Please cite this article as doi: 10.1002/MRM.28572

Running Headline: Comparison of VSASL Schemes

Word Count: Text (5497), Abstract (242)

Keywords: arterial spin labeling, velocity selective, velocity selective saturation, velocity selective inversion, SNR efficiency, eddy current sensitivity

Abstract

Purpose: In velocity-selective arterial spin labeling (VSASL), strategies using multiple saturation modules or using VS inversion (VSI) pulse can provide improved signal-to-noise ratio (SNR) efficiency compared to the original labeling scheme using one VS saturation (VSS) module. Their performance improvement, however, has not been directly compared.

Methods: Different VS labeling schemes were evaluated by Bloch simulation for their SNR efficiency, eddy current (EC) sensitivity and robustness against B_1 and B_0 variation. These schemes included dual-module double-refocused hyperbolic secant and symmetric 8-segment B_1-insensitive rotation (sBIR8-) VSS pulses, the original and modified Fourier-Transform-based VSI pulses. A subset of the labeling schemes was examined further in phantom and in vivo experiments for their EC sensitivity and SNR performance. An additional sBIR8-VSS with a built-in inversion (sBIR8-VSS-inv) was evaluated for the effects of partial background suppression (BGS) to allow a fairer comparison to VSI.

Results: According to the simulations, the sBIR8-VSS was the most robust against field imperfections, and had similarly high SNR efficiency (dual-module, dual-sBIR8-VSS) compared with the best VSI pulse (sinc-modulated, sinc-VSI). These were confirmed by the phantom and in vivo data. Without additional BGS the sinc-VSI pulses had the

highest temporal SNR, closely followed by the sBIR8-VSS-inv pulse, both benefitted from partial BGS effects.

Conclusion: Dual-sBIR8-VSS and sinc-VSI measured the highest SNR efficiency among the VS labeling schemes. Dual-sBIR8-VSS was the most robust against field imperfections while sinc-VSI may provide a higher SNR efficiency if its immunity to field imperfections can be improved.

Keywords: arterial spin labeling, velocity selective, velocity selective saturation, velocity selective inversion, SNR efficiency, eddy current sensitivity

1. Introduction

Arterial Spin Labeling (ASL) is a powerful technique to measure perfusion without the use of contrast agents (1, 2). Many variants have been developed since its inception to overcome many technical challenges it exhibits. While pseudo-continuous ASL (PCASL) (3) is the dominant technique accepted by the community for perfusion imaging in the brain (4), it still faces some challenges such as bolus arrival time effects (5-8) and variability in labeling efficiency (9, 10). New developments in velocity-selective (VS) labeling pulses represent a viable alternative to pseudo-continuous labeling (11-17). Primarily, VS pulses are much less sensitive to variations in bolus arrival times and they do not require a specific location in the vasculature for labeling. VS pulses also allow for faster repetition times and are thus beneficial for perfusion-based functional MRI (16, 18).

Velocity-selective pulses fit into two categories: VS saturation pulses (VSS) and VS Inversion (VSI) pulses. VSS pulses tip the magnetization into the transverse plane briefly before tipping it back to the longitudinal axis. A combination of RF and gradient pulses can be used to dephase the magnetization of spins traveling above a given cutoff velocity (V_{cut}) during the process. These fast-moving spins are effectively saturated through the mixing effect given a laminar flow distribution. The last segment in a VSS pulse tips the magnetization back to the longitudinal axis (12, 14, 17). Under the control condition, all the spins are tipped down to the transverse plane and then back to

the longitudinal axis without dephasing, so the magnetization remains unperturbed except for the same relaxation effects as under the label condition. Fourier-transform based VSI (FT-VSI) pulses consist of velocity encoding RF and gradient pulses that will only invert the spins traveling at the selected velocity (typically near zero). Under the control condition in VSI, all spins are inverted (11, 15, 19).

In theory, VSI pulses should yield nearly twice as much ASL signal as VSS pulses, but they are more sensitive to imperfections in B_1, B_0 and to eddy current (EC) effects than BIR8-based VSS pulses. On the other hand, multiple VSS modules can be concatenated to produce a larger bolus of label and hence a stronger ASL signal while being less sensitive to B_1, B_0 variations and EC effects (13) than VSI pulses.

In this work we aim to compare the performance of multiple variants of VSASL pulses and labeling schemes. Among these variants, we explore the original FT-VSI pulses as well as three new variants with improved velocity profiles. Our analysis also included the double-refocused hyperbolic secant (DRHS-) VSS pulse (12), the original symmetric BIR8 (sBIR8-) VSS pulse (17), a sBIR8 variant that inverted the stationary spins (13), and a combination of two consecutive sBIR8 VSS pulses (13). We compare the performance of these pulses to PCASL, which is the accepted standard ASL technique.

2. Methods

2.1 Bloch Simulations

FT-VSI pulses can be sensitive to B_0 and B_1 errors (15), similar as some earlier VSS based pulses (12, 20), except the BIR-based pulses (14, 17, 21). We simulated the evolution of an isochromat experiencing each of the velocity-selective labeling pulses over -100 and 100 cm/s and recorded the longitudinal magnetization response. The pulses included: 1) single-module VSS with DRHS pulse (DRHS-VSS) as implemented in (12); 2) dual-module VSS with DRHS (dual-DRHS-VSS) (13); 3) single-module VSS with sBIR8 pulse (sBIR8-VSS) (17); 4) dual-module VSS with sBIR8 (dual-sBIR8-VSS) (13); 5) original VSI sequence with rectangular small flip-angle RF pulses (rect-VSI) (15); 6) a modified VSI pulse using maximum-phase sinc modulation (mp-sinc-VSI) (22); and

two new modified VSI pulses using 7) a segmented sinc pulse as the small flip-angle RF pulses (segmented-sinc-VSI); and 8) a regular sinc modulation (sinc-VSI) on the rectangular small flip-angle RF pulses (**Figure 1**). The two new modified VSI pulses were designed to provide improved velocity profiles and B_1 robustness. Specifically, the segmented-sinc-VSI pulse was constructed by subdividing a 180°, single-lobed sinc pulse into 9 pieces of equal duration. In contrast, the sinc-VSI pulse was constructed by concatenating 9 rectangular pulses with a single-lobed sinc modulation (the amplitude of the nth pulse is given by $\text{sinc}(n\pi/5 - \pi)$, where n = 1, 2, …, 9). The flip angles of these 9 rectangular pulses add up to 180°. Some of the timing parameters of the VS pulses can be found in **Table 1.** Under the control condition, the VS gradients were set to 0 so that the V_{cut} was effectively infinity. The longitudinal magnetization under both labeling and control conditions were simulated and subtracted to yield the ASL signal.

2.1.1 Calculation of the cutoff velocity

The V_{cut} refers to the minimum velocity of the blood required for labeling to occur. It plays a crucial role in VS labeling because 1) it determines the amount of arterial spins available for labeling, i.e., the size of the labeling bolus; 2) it determines the weighting of tissue perfusion vs. intravascular signal in the measurement; 3) it also determines how close the label is to the destination tissue (or capillary bed). Given that the velocity profiles of these techniques are so different, we need a definition of V_{cut} that is equivalent, to have a fair comparison for both the saturation- and inversion-based labeling methods.

In order to define V_{cut}, we assume that the arterial spins of interest have a laminar flow pattern and their longitudinal magnetization is a function of the mean velocity after experiencing a VS pulse (12, 23). We define the V_{cut} as the point where ASL signal (Sig_{ASL}, defined as the magnetization difference between the signals in the selective and non-selective cases, relative to the relaxed magnetization) equals 1 in both the saturation and inversion schemes. Note that this is the first zero-crossing point under the label condition for saturation as in its original definition.

With this definition, the population of labeled spins is matched for both VSS and VSI. The same V_{cut} can be used in vascular crushing in the imaging, enabling accurate quantification and reducing contamination from venous contribution. A V_{cut} of 2 cm/s was used throughout this study. The Sig_{ASL} vs. V_{mean} profiles and corresponding V_{cut} are demonstrated in **Figure 2A** for both VSS and VSI.

To provide more realistic estimation on the overall labeling efficiency, we used the measured population distribution of arterial blood moving at different mean velocities at labeling from a previous brain perfusion study (24) (linearly interpolated within 2 - 96 cm/s with a step size of 2 cm/s, shown in **Figure 2B**) to weight the ASL signals at different mean velocities, e.g., those in **Figure 2A**. The overall ASL signal was calculated by summing up the ASL signal at different mean velocities with such weights to account for the effective population available for labeling and its SNR efficiency (i.e., SNR per unit time, defined as $Sig_{ASL}/\sqrt{2TR}$) was then calculated accordingly.

2.1.2 B_1 and B_0 sensitivity simulation

In a series of simulations, B_1 was scaled by a factor from 70% to 130% of its nominal value with an interval of 10%, and B_0 (off-resonance) was varied from -200 to +200 Hz with an interval of 50 Hz. For simulating the overall performance on a labeling volume in practical scenarios, the variation of B_1 and B_0 was assumed to have a 2D Gaussian distribution (μ_{B1} = 100%, σ_{B1} = 30%, μ_{B0} = 0, σ_{B0} = 200 Hz, ρ = 0). The results were then averaged across the B_1 and B_0 variation with the Gaussian weighting.

The sBIR8-VSS pulse with a nominal B_1 (100%) and no off-resonance was considered as the reference for comparison due to its insensitivity to B_1 and B_0 variation (17). The results were normalized to this reference. To examine the VS pulses' sensitivity to B_1 and B_0 variation thus the labeling efficiency loss, an additional labeling efficiency term β was calculated by dividing the average signal across the B_1 and B_0 variation by that without any variation. Other parameters used in the simulations included: T_1 = 1660 ms, T_2 = 150 ms, TR = 4500 ms, TI (single-module) = 1300 ms, TI_1/TI_2 (dual-module) = 1150/820 ms. Imaging time was ignored. Additionally, for the dual-module case, the condition $TI_1 + TI_2$ < bolus duration was assumed (13).

2.1.3 Eddy current effects simulation

Typically, strong velocity-sensitive gradient pulses are used in combination with short delays between RF and gradient pulses to reduce the T_2 relaxation during the labeling process. Eddy currents are generated by these gradient pulses, and can interfere with the labeling pulses, having different effects on the spins under the labeling and control conditions. If not properly accounted for, the EC effects can generate spurious "ASL" signals and compromise the quantification accuracy in VSASL (14, 17). To investigate the sensitivity to the EC effects, Bloch simulations were performed for these different VS pulses following the methods in (14, 17) with EC amplitude of 0.25% and time constants of 0.1 to 1000 ms. A nominal B_1 and B_0 = 0 Hz and gradient pulses with a ramp time of 0.3 ms and a maximum amplitude of 30 mT/m were used. No relaxation effect was considered.

2.2 Phantom experiments

The EC sensitivity of different VS labeling pulses was evaluated in a spherical phantom filled with agar (25) on a 3.0 Tesla, MR750 scanner (General Electric, Milwaukee, WI, USA) using a 32-channel receive coil (Nova Medical, Wilmington, MA, USA). Four VS labeling schemes with the same parameters as in the Bloch simulation were tested: sBIR8-VSS, rect-VSI, segmented-sinc-VSI and sinc-VSI. The images under the label and control conditions were collected 400 ms after the application of the VS pulses. The VS gradient pulses were applied along the S/I direction. The signals under the control condition were used as the reference. The signal difference between the label/control conditions was calculated and then normalized to the reference signal to give a subtraction error as an indicator for the EC sensitivity. Note that the T_2 relaxation was compensated in this process.

2.3 In vivo experiments

Healthy participants (N=9) were scanned on the same scanner, according to the guidelines of the University of Michigan's Internal Review Board, including informed

consent. Each participant received seven ASL scans using the same readout module, but different labeling schemes.

The readout module consisted of a multi-echo, stack-of-spirals 3D readout. The imaging parameters can be found in the Supporting Information. No additional background suppression (BGS) (26) pulses were used with any of the schemes, because we intended to directly compare the ASL signal intensity without the confounding effects of BGS pulses (please see discussion). The first pair in the series was not preceded by any labeling pulses and was used as the reference image (proton density). A sBIR8 VSS pulse with the same V_{cut} in labeling was applied 100 ms prior to readout in order to suppress the arterial compartment's contribution to the ASL signal.

We tested a subset of the labeling schemes simulated in the above section. The labeling schemes were: 1) PCASL: pseudo-continuous ASL as recommended in the consensus paper (label duration = 1800 ms and post-label delay (PLD) = 2000 ms) (4) following a quick phase calibration scan to compensate for off-resonance effects in the labeling region (9, 10); 2) rect-VSI; 3) segmented-sinc-VSI; 4) sinc-VSI; 5) sBIR8-VSS: a single-module sBIR8-VSS pulse; 6) sBIR8-VSS-inv: identical to the sBIR8-VSS pulse, but with an additional phase of π on the last RF segment in the sBIR8 scheme to invert the magnetization of stationary spins (13), for a fairer comparison to the VSI pulses with partial BGS effects; 7) dual-sBIR8-VSS: the dual-module sBIR8-VSS pulse with TI_1/TI_2 = 1150/820 ms. The pulses were identical to those in the Bloch simulation.

The velocity encoding gradient amplitude in all velocity-selective pulses was chosen such that the V_{cut} was 2 cm/s along the S/I direction and the PLD was 1400 ms, unless otherwise specified.

2.4 In vivo data processing

Two subjects were excluded in the in vivo analyses due to overall poor image quality with multiple labeling schemes, especially with PCASL. The control and labeled images were pairwise subtracted and averaged over the time course for each scan. Diffusion

attenuation correction (13) was performed on the VSASL signals. The b-values of the sBIR8-VSS pulse was calculated to be 0.37 s/mm^2, and the b-values of 0.2 s/mm^2 (15) was used for the VSI pulses. Images of the percentage signal change relative to the spin density image were then calculated. The temporal standard deviation (SD) of the ASL subtraction images was calculated and used to calculate temporal SNR (tSNR) images. The resulting images were evaluated for quality and the presence of obvious artifacts.

CBF maps were computed from the ASL difference images using a single-compartment kinetic model (27) adapted for each respective labeling scheme. Specifically for VS labeling methods, the labeling efficiency term was adjusted for the T_2 relaxation during labeling, $\alpha = e^{-eTE/T_{2a}}$, and an additional labeling efficiency term β (**Table 1**) for the labeling efficiency loss due to B_1 and B_0 variation.

GM masks were constructed based on the average ASL signal maps across all the modalities in each subject. The mean ASL signal, tSNR and CBF in the GM region of interest (ROI) were calculated and compared between different labeling schemes. We also investigated the agreement in ASL signals between each VS labeling scheme and PCASL, by fitting a linear model and calculating the correlation coefficient, slope and intercept over each subject's voxels in the whole brain.

2.5 Statistical analysis

Jarque-Bera tests were carried out on the mean ASL signal, tSNR and CBF in the GM ROI across subjects and confirmed the normality of the distribution. One-way ANOVA and multiple pairwise comparison tests (Bonferroni corrected) were then performed to detect if there was any significant difference between any pair of the labeling schemes with $p < 0.05$, and similarly, on the results of the correlation analysis.

3. Results

The Bloch simulation results are shown in **Figures 3** and **4**. Between the two VSS pulses, the sBIR8-VSS pulse gave robust cosine-shaped responses vs. velocity across the large ranges of B_1 and B_0 variation examined, and showed less sensitivity to EC effects, as reported previously (17). Among the four VSI pulses, the rect-VSI and the segmented-sinc-VSI pulses showed significant sensitivity to both B_1 and B_0 variation, demonstrated by the degraded magnetization response when B_1 was off from the nominal value and the tilted inversion bands when the off-resonance increased. Both of them also showed considerable EC sensitivity. In addition, the rect-VSI pulse showed oscillating magnetization response in the velocity passband as reported previously (15); while the segmented-sinc-VSI pulse had smooth response in the velocity passband, though the performance degraded quickly when the off-resonance increased. The mp-sinc-VSI showed improved performance against B_1 and B_0 variation (22) and EC effects, with slight oscillations in the velocity passbands. The sinc-VSI demonstrated the most robust performance against B_1 and B_0 variation among the four VSI pulses, as well as having smooth magnetization response across the velocity passbands. The sinc-VSI pulse also showed the least sensitivity to EC effects among all the six VS pulses studied by simulation. Note that though the magnetization response in **Figure 3** showed different velocity profiles under the label condition, they all had the same matched V_{cut} as defined previously. Another interesting finding was that all the VSI pulses showed spatially oscillating EC sensitivity, while the VSS pulses had relatively smooth EC sensitivity across space.

After weighting the ASL signal profiles (with T_2 relaxation) with the measured arterial blood mean velocity distribution (**Figure 2B**), the SNR efficiencies of the labeling pulses were calculated at different B_1 and B_0 offsets and are shown in **Figure 5**. The dual-sBIR8-VSS pulse showed excellent robustness to both B_1 and B_0 variation as expected, especially with a strong B_1 field.

All the VSI pulses studied showed various sensitivities to B_1 and B_0 variation. The segmented-sinc-VSI pulse had slightly improved B_1 insensitivity compared to the rect-VSI pulse; however, it was more susceptible to B_0 variation. Both mp-sinc-VSI and sinc-VSI pulses improved the overall performance, with the sinc-VSI pulse being slightly

better. Comparing to the sinc-VSI pulse, the dual-sBIR8-VSS pulse provided very good insensitivity to B_1 and B_0 variation, though the maximal SNR efficiency was lower than that with the sinc-VSI pulse under ideal conditions.

Averaged across the B_1 and B_0 variation with the aforementioned Gaussian distribution, the overall SNR efficiency was calculated for each labeling strategy and is listed in **Table 1**. Please note that the SD was calculated without the Gaussian weighting. Using the sBIR8-VSS pulse as the reference, the dual-sBIR8-VSS, the mp-sinc-VSI and the sinc-VSI pulses gained over 30% SNR efficiency increase. The dual-sBIR8-VSS had the most consistent SNR efficiency with the smallest SD. The rect-VSI pulse only showed a 18.1% increase compared to the sBIR8-VSS, or 26.4% when compared with the single-module DRHS pulse, in agreement with the results reported previously (15). The sinc-VSI performed the best with a 37.8% overall increase in SNR efficiency among all the labeling methods, though with a relatively large SD value. sBIR8-VSS reported the highest β of 0.983 among all, followed by 0.922 with DRHS; while sinc-VSI reported the highest β of 0.881 among the VSI pulses and closely followed by the mp-sinc-VSI, and the segmented-sinc-VSI had the lowest β of 0.609.

The subtraction error maps on the phantom are shown in **Figure 6** to demonstrate the EC sensitivity of the VS labeling pulses. The root mean squared percentage signal difference over the whole volume was: 0.19% for sBIR8-VSS, 0.44% for rect-VSI, 0.35% for segmented-sinc-VSI, and 0.23% for sinc-VSI. Both the sBIR8-VSS and the sinc-VSI pulses were robust against the EC effects, showing similar and negligible subtraction errors; while the rect-VSI and segmented-sinc-VSI pulses had much higher subtraction errors, or EC sensitivity. In addition, the concentric ring patterns of the errors demonstrated the spatial oscillation of the EC sensitivity of the VSI pulses, confirming the Bloch simulation results shown earlier.

The in vivo results are shown in **Figure 7** and **Table 2.** The ASL signal is the voxelwise difference between selective and non-selective images, expressed as a percentage of the spin density image. The temporal SNR is the voxelwise time-averaged signal difference divided by its SD. Comparing to PCASL, most of the VS labeling produced

similar blood flow patterns. However, there were errors with the segmented-sinc-VSI and the rect-VSI labeling. As demonstrated by the example shown in **Figure 7A**, the ASL signals in the right frontal regions with the segmented-sinc-VSI pulse were spuriously reduced; the rect-VSI showed strong "artificial" ASL signal in some regions while having reduced ASL signal in others. These errors were likely due to the B_0 or EC sensitivity of these pulses, and were consistent with the simulation and phantom results reported earlier. Note that the ASL signal artifacts from the ASL signal maps were carried into the tSNR maps, e.g., the erroneous ASL signal with rect-VSI artificially increased the tSNR regionally. There were artifacts shown as negative ASL signals close to the base of brain, likely due to flow fluctuation or motion in general, and should be reduced by BGS.

Across subjects, statistically significant difference in the ASL signal was detected by the ANOVA test ($F = 3.22$, $P = 0.011$), but the pairwise comparison tests only detected a strong trend that the sBIR8-VSS-inv had a lower signal than PCASL ($P = 0.052$). The rest of the pairwise comparisons were not statistically significant ($P > 0.126$). On average, PCASL labeling produced the highest GM ASL signal (0.648 ± 0.062%) among all. Though the rect-VSI reported the second highest GM ASL signal (0.630 ± 0.097%, a 26.8% increase compared to sBIR8-VSS), some of the contribution was likely from the erroneous EC effects, as pointed out earlier. The sinc-VSI and dual-sBIR8-VSS pulses produced artifact-free ASL images with very similar GM ASL signal (0.620 ± 0.093% and 0.618 ± 0.111%, respectively), demonstrating improvement compared to single-module VSS pulse, though not as much as predicted by the simulation (24.8% vs. 37.8% for sinc-VSI, and 24.4% vs. 31.5% for dual-sBIR8-VSS). The measured signal improvement with dual-sBIR8-VSS was comparable with that in a previous in vivo study (22.1%) (13). Surprisingly, the segmented-sinc-VSI showed a 16.3% increase of signal compared to sBIR8-VSS pulse, higher than the predicted value of -4.2%.

The tSNR maps and averaged values in **Figure 7 and Table 2** showed that the tSNR was significantly higher with the VSI methods (3.188 ± 0.814, 2.798 ± 0.763 and 2.874 ± 0.772 for rect-VSI, segmented-sinc-VSI and sinc-VSI, respectively) due to the built-in inversion on the brain tissue. One-way ANOVA tests of the tSNR across the different

labeling schemes yielded significance differences between the schemes (F = 14.74, $P = 5.63 \times 10^{-9}$). Multiple pairwise comparison tests (Bonferroni corrected) between the schemes showed that difference between each of the VSI schemes and most of the VSS schemes (except sBIR8-VSS

-inv), as well as PCASL, was significant ($P < 1.34 \times 10^{-3}$). However, the tSNR of the sBIR8-VSS-inv scheme was not significantly different from any of the VSI schemes ($P > 0.27$). The sBIR8-VSS-inv scheme had statistically significantly higher tSNR than the sBIR8-VSS and PCASL schemes ($P = 0.012$ and 0.021, respectively), but had comparable tSNR with the dual-sBIR8-VSS ($P = 0.11$). We attribute this improvement in tSNR to the partial BGS produced by inverting the magnetization of the whole volume prior to acquisition. Indeed, comparing the sBIR8-VSS labeling and sBIR8-VSS-inv, we found that the built-in inversion improved the tSNR by 2.4-fold on average (from 0.926 ± 0.291 to 2.258 ± 0.645), even though the ASL signal is expected to be identical in theory. The tSNR of dual-sBIR8-VSS (1.207 ± 0.547) was significantly lower than those of VSI pulses ($P < 1.34 \times 10^{-3}$), but comparable with the sBIR8-VSS-inv pulse.

Comparing the CBF maps shown in **Figure 7A**, in addition to the similar spatial variation (including the artifacts) observed in the ASL signal maps, we also observed lower values with sinc-VSI labeling and higher values with dual-sBIR8-VSS labeling in this subject. The averaged GM CBF values were in expected range for all the labeling schemes in each subject. At the group level, no statistically significant difference was detected in the GM CBF with different labeling schemes by the ANOVA test (F = 2.00, $P = 0.087$), and the multiple pairwise comparison tests only found that the sinc-VSI tended to have lower GM CBF values compared to dual-sBIR8-VSS ($P = 0.138$), consistent with the observation in the exemplary CBF maps.

The results of the linear regression and correlation analyses of the ASL signal in the whole brain can be found in the Supporting Information.

4. Discussion

We have compared currently available VS labeling strategies with respect to their SNR efficiency and robustness against field imperfections, such as B_1 and B_0 and EC effects. The simulation, phantom and in vivo experiments showed consistent results. Overall, the dual-sBIR8-VSS pulse were the most robust VS labeling strategy against B_1 and B_0 variation and EC effects according to the Bloch simulation and phantom experiments, respectively, while sinc-VSI were slightly more sensitive to B_1 variation. Both dual-sBIR8-VSS and sinc-VSI had comparably high ASL signal in vivo.

In this study, we have extended the definition of V_{cut} for VSS to the VSI pulses in a practical manner. It is a critical imaging parameter in VS labeling for the reasons mentioned earlier. In addition, it is important to match the V_{cut} in both labeling and imaging for perfusion quantification accuracy, as well as reducing contamination from the venous compartment, which can be generally filtered out by the velocity-selective criterion set by the V_{cut} in imaging due to acceleration. It is clearly defined and matched for VSS labeling as the flow crushing in imaging relies on the same dephasing effect. With the extended definition of V_{cut}, it is now possible to have a matched bolus of label delivered and imaged with VSI labeling. As shown in **Figure 3**, though the magnetization vs. velocity profiles may appear very different for VSS and VSI initially, after considering the laminar flow mixing effect and correctly setting the flow sensitive gradient strength, the “cut-off” effect is almost identical (**Figure 2A**), therefore VSS and VSI labeling can be compared in a fairer and more quantitatively accurate manner.

The sBIR8-VSS pulse showed excellent robustness against B_1 and B_0 variation, and EC effects. With the dual-module preparation, the SNR efficiency improvement was consistently high, as reported previously (13). These benefits are mainly adopted from the BIR pulse train and the symmetric layout of the gradient pulses (17). The VSI pulses, on the other hand, use hard RF pulses to tip and refocus the magnetization during velocity encoding. These RF pulses are inherently B_1 sensitive. There has been research showing improved B_1 behavior by using composite 180° refocusing pulses, in combination of MLEV phase cycling pattern, and/or modulation on the small tipping RF pulses (28-30), including the proposed sinc modulation in this study. These modifications improved the robustness against B_1 and B_0 variation to some extent;

however, the B_1 sensitivity remains one of the main factors affecting the labeling efficiency for VSI. Under ideal conditions, VSI pulses should provide higher SNR efficiency than dual-module VSS labeling; however, due to the sensitivity to field imperfections (mainly B_1), the VSI pulses currently yielded comparable ASL signal with dual-sBIR8-VSS labeling. Future research should be focusing on improving the B_1 insensitivity for VSI pulses.

Additional BGS pulses were deliberately not applied, because their effects are relatively independent of the labeling process, but would interfere with the measurement of labeling efficiency. Although BGS is crucial in reducing the noise in ASL, to reach the same degree of BGS, different number of BGS pulses have to be applied for the VSI and VSS pulses, such as in (15). Then the inversion efficiency of the BGS pulses has to be accurately measured in each subject to correct for their effects on the ASL signal, which would likely introduce additional biases.

At the same time, the VSI pulses themselves invert the tissue magnetization and thus inherently suppress the background signal to some extent and had boosted the tSNR. This is not the case in VSS or PCASL, for example, the tSNR with PCASL was low due to the absence of BGS. Therefore, the sBIR8-VSS-inv pulse was used to effectively achieve a similar partial BGS and thus disambiguate the effects of labeling efficiency and partial BGS. Indeed, the in vivo results comparing the sBIR8-VSS pulse with and without the built-in inversion clearly demonstrated the importance of BGS in improving the tSNR, thus the necessity of using BGS techniques if possible. For example, if a similar improvement of tSNR can be realized by a built-in inversion with the dual-sBIR8-VSS scheme, its tSNR would be about 2.94, comparable with those measured by VSI labeling schemes. In this study, the effect of BGS on tSNR was not simulated because this effect is independent of the labeling preparation, i.e., similar levels of BGS can be achieved with additional BGS pulses for any labeling pulses. Under perfect BGS conditions, the tSNR is then mainly determined by the ASL signal intensity generated by a given labeling preparation. There are practical considerations for implementation, such as constraints on specific absorption rate (SAR), timings of BGS pulses, etc. One

example is that the sBIR8-VSS-inv pulse provided some level of BGS and a significant tSNR gain without SAR increase.

It was interesting to observe that the EC sensitivity of the pulses were well matched between the simulation, the phantom and the in vivo experiments. The artificial ASL "signal" (or signal void) shown in **Figure 7A** signified the necessity for a good EC compensating pulse design in VS labeling (14, 17). With the sinc modulation on VSI pulse, the EC sensitivity was further reduced compared to the sBIR8-VSS pulse. The two pulses had similar subtraction error in the phantom experiments. This may be because the subtraction error likely included B_1 and B_0 sensitivity effects, whereas in the EC sensitivity simulation, the B_1 and B_0 sensitivity was ignored. The spatial fluctuation of the EC sensitivity of the VSI pulses predicted by simulation were also reported previously (15), and was observed in phantom experiments in this study. The spatially smooth EC sensitivity of the sBIR8-VSS pulse was observed in the phantom experiments, consistent with the simulation prediction. Only the EC sensitivity data along the S/I direction were collected on phantom as this is the most relevant velocity encoding direction in a typical ASL experiment in the brain.

The effective TE (eTE) of the VSS and VSI labeling pulses is determined by the time the spins spent effectively on the transverse plane. In turn, it determines the arterial signal relaxation during the labeling process. The shorter the eTE, the higher the labeling efficiency for VS labeling. As shown in **Table 1**, the eTE of the VSI pulses were not dramatically increased even though the total pulse duration increased by two- to three-fold compared with the VSS pulses. This is a desirable property for the VSI pulses as the small flip-angle pulses tip the magnetization through the transverse plane continuously during the entire labeling process. Proper modulation of these small flip-angle pulses, e.g., those in (29, 30) and the sinc modulation in this study, can be explored further to find a design with a good B_1 robustness and a short eTE for a high labeling efficiency.

In this study, the ranges of the B_1 and B_0 variation were within the values observed in practice. Unlike pulsed ASL (PASL) or PCASL, the labeling region in VSASL is "global",

i.e., the full covered volume of the transmitting RF coil. It is expected to have more variation in both B_1 and B_0 fields than that would be seen for PASL or PCASL in the labeling region. Therefore, it is more critical to have a VS labeling pulse with sufficient immunity to field imperfections, including the EC effects. We used a (an arbitrary) Gaussian distribution of the variation to evaluate the overall SNR efficiency for these VS pulses under a more practical setting and had derived the additional labeling efficiency term β to summarize these effects. The simulation results matched relatively well with the experimental results regarding the ASL signal in this study, for example, the predicted SNR improvement of the rect-VSI pulse over the DRHS pulse matched with that measured in vivo in another study (26.3% vs ~30% after correction for BGS effects) (15). However, there were also discrepancies regarding the value of β, especially when applied in CBF quantification. For example, the sinc-VSI tended to underestimate CBF when compared with PCASL, indicating a lower β with our current implementation. Similarly, rect-VSI might also have a lower β than the predicted value of 0.727. This was consistent with the calculated β of 0.67 in another in vivo study (15). On the other hand, the β values yielded comparable GM CBF values with PCASL for segmented-sinc-VSI and sBIR8-based labeling schemes. These discrepancies call for further investigation on the β with respect to the implementation of VS labeling in practice. Even though PCASL was used as the reference method in this study, it can have variable labeling efficiency in individuals or in different supplying arteries, a labeling method with a more stable labeling efficiency, such as PASL, may be more suitable for this purpose.

There were several limitations of this study: 1) the in vivo scans always followed the same acquisition order. This might produce some small bias, due to habituation effects or change of alertness levels. However, previous test-retest reproducibility measurements of brain perfusion using ASL (31, 32) suggest that this bias might not be a significant factor; 2) the normalized mean velocity population distribution (**Figure 2B**), though being the best approximation available at the time, contains its own uncertainty and thus might affect the accuracy of the overall ASL signal estimation; 3) since additional BGS pulses were deliberately not used, the physiological noise affects the uncertainty (variance) of the in vivo results, especially for the PCASL and sBIR8-VSS based scans. Alternatively, an ideal comparison could be made between the VSI pulses

and the dual-sBIR8-VSS pulse with the second module being sBIR8-VSS-inv, both with the same number of additional BGS pulses and the same degree of BGS.

5. Conclusion

In this study, we had compared currently available VS saturation and inversion labeling strategies, including dual-module VSS and different variants of VSI pulses. Their SNR efficiency and robustness against B_1, B_0 and EC effects were evaluated through Bloch simulation, phantom and human experiments. Both dual-sBIR8-VSS and sinc-VSI measured the highest SNR efficiency in vivo among the VS labeling schemes investigated. Overall, the dual-sBIR8-VSS pulse was the most robust VS labeling strategy against field imperfections. While the sinc-modulated VSI pulse showed greater tSNR and was the best among the VSI methods, further technical improvement, such as improved robustness against B_1 variation, is needed to fully utilize its inversion labeling advantage for a higher SNR efficiency than the VSS labeling, as well as a better estimation of β in practice for accurate quantification. In addition, a proper BGS is crucial in improving the tSNR in VSASL scans, and should be applied if possible.

Acknowledgments

We thank Drs. Eric Wong and Divya Bolar for helpful discussion.

References

1. Detre JA, Leigh JS, Williams DS, Koretsky AP. Perfusion imaging. Magn Reson Med. 1992;23(1):37-45.

2. Williams DS, Detre JA, Leigh JS, Koretsky AP. Magnetic resonance imaging of perfusion using spin inversion of arterial water. Proc Natl Acad Sci U S A. 1992;89(1):212-6.

3. Dai WY, Garcia D, de Bazelaire C, Alsop DC. Continuous Flow-Driven Inversion for Arterial Spin Labeling Using Pulsed Radio Frequency and Gradient Fields. Magn Reson Med. 2008;60(6):1488-97.

4. Alsop DC, Detre JA, Golay X, Gunther M, Hendrikse J, Hernandez-Garcia L, et al. Recommended implementation of arterial spin-labeled perfusion MRI for clinical applications: A consensus of the ISMRM perfusion study group and the European consortium for ASL in dementia. Magn Reson Med. 2015;73(1):102-16.

5. Alsop DC, Detre JA. Reduced transit-time sensitivity in noninvasive magnetic resonance imaging of human cerebral blood flow. J Cereb Blood Flow Metab. 1996;16(6):1236-49.

6. Gonzalez-At JB, Alsop DC, Detre JA. Cerebral perfusion and arterial transit time changes during task activation determined with continuous arterial spin labeling. Magn Reson Med. 2000;43(5):739-46.

7. van Osch MJ, Hendrikse J, van der Grond J. Sensitivity comparison of multiple vs. single inversion time pulsed arterial spin labeling fMRI. J Magn Reson Imaging. 2007;25(1):215-21.

8. Zhou J, van Zijl PC. Effect of transit times on quantification of cerebral blood flow by the FAIR T(1)-difference approach. Magn Reson Med. 1999;42(5):890-4.

9. Jahanian H, Noll DC, Hernandez-Garcia L. B0 field inhomogeneity considerations in pseudo-continuous arterial spin labeling (pCASL): effects on tagging efficiency and correction strategy. NMR Biomed. 2011;24(10):1202-9.

10. Shin DD, Liu TT, Wong EC, Shankaranarayanan A, Jung Y. Pseudocontinuous arterial spin labeling with optimized tagging efficiency. Magn Reson Med. 2012;68(4):1135-44.

11. Norris DG, Schwartzbauer C. Velocity Selective Radiofrequency Pulse Trains. J Magn Reson. 1999;137:231-6.

12. Wong EC, Cronin M, Wu W-C, Inglis B, Frank LR, Liu TT. Velocity-selective arterial spin labeling. Magn Reson Med. 2006;55(6):1334-41.

13. Guo J, Wong EC. Increased SNR efficiency in velocity selective arterial spin labeling using multiple velocity selective saturation modules (mm-VSASL). Magn Reson Med. 2015;74(3):694-705.

14. Meakin JA, Jezzard P. An optimized velocity selective arterial spin labeling module with reduced eddy current sensitivity for improved perfusion quantification. Magn Reson Med. 2013;69(3):832-8.

15. Qin Q, van Zijl PC. Velocity-selective-inversion prepared arterial spin labeling. Magn Reson Med. 2016;76(4):1136-48.

16. Hernandez-Garcia L, Nielsen JF, Noll DC. Improved sensitivity and temporal resolution in perfusion FMRI using velocity selective inversion ASL. Magn Reson Med. 2019;81(2):1004-15.
17. Guo J, Meakin JA, Jezzard P, Wong EC. An optimized design to reduce eddy current sensitivity in velocity-selective arterial spin labeling using symmetric BIR-8 pulses. Magn Reson Med. 2015;73(3):1085-94.
18. Wu WC, Wong EC. Feasibility of velocity selective arterial spin labeling in functional MRI. J Cereb Blood Flow Metab. 2007;27(4):831-8.
19. de Rochefort L, Maitre X, Bittoun J, Durand E. Velocity-selective RF pulses in MRI. Magn Reson Med. 2006;55(1):171-6.
20. Wong EC, Liu TT, Sidaros K, Frank LR, Buxton RB, editors. Velocity selective arterial spin labeling. Proceedings of the 10th Annual Meeting of ISMRM; 2002; Honolulu, HI, USA. p621.
21. Wong EC, Guo J, editors. BIR-4 based B1 and B0 insensitive velocity selective pulse trains. Proceedings of the 18th Annual Meeting of ISMRM; 2010; Stockholm, Sweden. p2853.
22. Landes V, Jao T, Javed A, Nayak K, editors. Improved velocity-selective labeling pulses for myocardial ASL. Proceedings of the 27th Annual Meeting of ISMRM; 2019; Montréal, QC, Canada. p4967.
23. Wu W, Wong E. Intravascular effect in velocity-selective arterial spin labeling. Conf Proc IEEE Eng Med Biol Soc. 2005;6:5790-3.
24. Ding D, Guo J, Wong EC, editors. Measurement of Arterial Blood Velocity Distribution in the Human Brain Using Velocity Selective ASL. Proceedings of the 18th Annual Meeting of ISMRM; 2010; Stockholm, Sweden. p1776.
25. Glover G. FBIRN Stability phantom QA procedures [Available from: https://docplayer.net/81514980-Fbirn-stability-phantom-qa-procedures.html.
26. Ye FQ, Frank JA, Weinberger DR, McLaughlin AC. Noise reduction in 3D perfusion imaging by attenuating the static signal in arterial spin tagging (ASSIST). Magn Reson Med. 2000;44(1):92-100.
27. Buxton RB, Frank LR, Wong EC, Siewert B, Warach S, Edelman RR. A general kinetic model for quantitative perfusion imaging with arterial spin labeling. Magn Reson Med. 1998;40:383-96.
28. Qin Q, Shin T, Schar M, Guo H, Chen H, Qiao Y. Velocity-selective magnetization-prepared non-contrast-enhanced cerebral MR angiography at 3 Tesla: Improved immunity to B0/B1 inhomogeneity. Magn Reson Med. 2016;75(3):1232-41.
29. Matson GB. Design strategies for improved velocity-selective pulse sequences. Magn Reson Imaging. 2017;44:146-56.

30. Landes V, Javed A, Jao T, Qin Q, Nayak K. Improved velocity-selective labeling pulses for myocardial ASL. Magn Reson Med. 2020. Epub ahead. DOI: 10.1002/mrm.28253

31. Chen Y, Wang DJ, Detre JA. Test-retest reliability of arterial spin labeling with common labeling strategies. J Magn Reson Imaging. 2011;33(4):940-9.

32. Steketee RME, Mutsaerts HJMM, Bron EE, van Osch MJP, Majoie CBLM, van der Lugt A, et al. Quantitative Functional Arterial Spin Labeling (fASL) MRI - Sensitivity and Reproducibility of Regional CBF Changes Using Pseudo-Continuous ASL Product Sequences. PLoS ONE. 2015;10(7).

Table 1

	DRHS-VSS	dual-DRHS-VSS	sBIR8-VSS	dual-sBIR8-VSS	rect-VSI	segmented-sinc-VSI	mp-sinc-VSI	Sinc-VSI
Pulse Duration (ms)	23.8	23.8*2	24.4	24.4*2	49.4	67.6	69.1	69.1
Effective TE (ms)	20.6	--	20.7	--	26.8	28.8	27.8	31.3
Averaged SNR efficiency (a.u.)	0.118 ± 0.011	0.152 ± 0.014	0.126 ± 0.003	0.165 ± 0.004	0.149 ± 0.041	0.120 ± 0.058	0.169 ± 0.024	0.173 ± 0.025
Normalized SNR efficiency	0.935 ± 0.084	1.209 ± 0.110	1.000 ± 0.026	1.315 ± 0.035	1.181 ± 0.329	0.958 ± 0.465	1.3453 ± 0.192	1.378 ± 0.202

Additional labeling efficiency term (β)	0.922	0.922	0.983	0.983	0.727	0.609	0.880	0.881

Table 1. The parameters, the signal-to-noise (SNR) efficiencies and the additional labeling efficiency terms (β) for the VS labeling schemes. These values were calculated based on Bloch simulation. The effective TE's of dual-DRHS-VSS and dual-sBIR8-VSS were not listed because the two VSS modules have different effects on different sub-groups of the labeled bolus. The signal-to-noise ratio (SNR) efficiency of sBIR8-VSS was used as reference for calculation of the normalized SNR efficiency. Note that the standard deviation of the averaged SNR efficiency (and the normalized values) was calculated without Gaussian weighting. The additional labeling efficiency terms (β) were used in cerebral blood flow quantification to account for the additional labeling efficiency loss due to field imperfection.

Table 2

	PCASL	**rect-VSI**	**segmented-sinc-VSI**	**sinc-VSI**	**sBIR8-VSS**	**sBIR-VSS-inv**	**dual-sBIR8-VSS**
Averaged signal (%) in GM	0.648 ± 0.062	0.630 ± 0.097	0.578 ± 0.102	0.620 ± 0.093	0.497 ± 0.096	0.472 ± 0.092	0.618 ± 0.111

Averaged tSNR in GM	0.989 ± 0.232	3.188 ± 0.814	2.798 ± 0.763	2.874 ± 0.772	0.926 ± 0.291	2.258 ± 0.645	1.207 ± 0.547
Averaged GM CBF (ml/100g/min)	51.5 ± 5.0	49.6 ± 7.7	55.1 ± 9.7	41.6 ± 6.3	55.6 ± 10.7	52.8 ± 10.3	56.1 ± 10.1

Table 2. The normalized ASL signal, temporal SNR (tSNR) and cerebral blood flow (CBF) in gray matter (GM), averaged across subjects (mean ± standard deviation). Significant differences in tSNR between the labeling schemes were detected and labeled in Figure 7B. No significant difference in ASL signal or GM CBF was detected between the labeling schemes.

List of Figures

Figure 1: The pulse diagrams of double-refocused hyperbolic secant (DRHS) velocity-selective saturation (VSS) pulse (DRHS-VSS)), symmetric BIR8 VSS (sBIR8-VSS) pulse, the original VSI pulse using hard RF pulses of the same small flip angles (rect-VSI), a modified VSI pulse with a regular sinc-shaped inversion pulse of 9 segments (segmented-sinc-VSI), a modified VSI pulse with a maximum-phased sinc modulation on the amplitude of the small flip-angle pulses (mp-sinc-VSI), and the modified VSI pulse with a regular sinc modulation (sinc-VSI).

Figure 2: (A) The Sig_{ASL}-V_{mean} profiles for the VSS and VSI labeling after convolving with a laminar flow distribution, showing the definition of the cutoff velocity (e.g. 2 cm/s); (B) the arterial blood population distribution obtained experimentally. Linear interpolation

was used to estimate the population over the range of 2 - 96 cm/s of mean velocity. Note the well-matched cut-off profiles between VSS and VSI pulses.

Figure 3: Simulated velocity response of the corresponding velocity selective labeling pulses in **Figure 1** under the label (solid red curves) and the control (dashed blue curves) conditions, with T_1 (1660 ms) and T_2 (150 ms) effects taken into consideration. No B_1 or off-resonance effects were considered for these simulations.

Figure 4: The simulation results showing the performance of the VS labeling pulses: (A) the magnetization vs. mean velocity response under the labeling condition showing the sensitivity to B_1 variation (ranging from 0.7 to 1.3 of the nominal value) without off-resonance; (B) the magnetization vs. mean velocity response under the labeling condition showing the sensitivity to B_0 variation (ranging from -200 Hz to 200 Hz) when B_1 = 1; (C) the magnetization of the static tissue (V = 0) under the label condition showing the eddy current (EC) sensitivity of the VSS and VSI pulses to EC components with different time constants (ranging from 0.1 ms to 1000 ms) at different distance to the iso-center of the magnet; where the magnetization under the control condition can be referred to the center line at distance = 0. Please note the different color scales for VSS and VSI pulses. The sBIR8-VSS pulse demonstrated strong immunity to B_1 and B_0 variation, and EC effects; while the sinc-VSI pulse had the highest robustness among the VSI pulses. Note that the response in panels A and B was generated before taking laminar flow effects into account.

Figure 5: The overall signal-to-noise (SNR) efficiency maps of different VS labeling strategies from simulation, showing their sensitivity to the B_1 and B_0 variation averaged over the arterial velocity distribution in the brain. Note that the sBIR8-VSS pulse had an excellent immunity to B_1 and B_0 variation, and the sinc-VSI pulse had the best

performance among the VSI pulses. The sinc-VSI pulse also had higher SNR efficiency when the B_1 and B_0 variation was not too large.

Figure 6: The subtraction error maps obtained from phantom scans, demonstrating eddy current (EC) sensitivity of the pulses. The velocity sensitive gradient pulses were applied in the S/I direction and the maps were normalized to the reference spin density image. The sBIR8-VSS and the sinc-VSI pulses showed comparable and low errors; while the rect-VSI and segmented-sinc-VSI had stronger sensitivity to EC effects with a spatially varying pattern.

Figure 7: (A) Comparison between labeling schemes on four slices from a representative subject, showing the relative signal change due to the label (left panel, normalized to the spin density image), the corresponding temporal SNR images for each of the techniques (middle panel) and the corresponding quantitative CBF maps (right panel); (B) the averaged ASL signal per voxel across subjects (left panel, normalized to the spin density image), the averaged temporal SNR per voxel across subjects (middle panel) and the averaged CBF values per voxel across subjects (right panel); where the red bars indicate the median values. The dual-sBIR8-VSS showed the greatest amount of signal. Note that the rect-VSI and the chopped VSI schemes contained artifacts with “spurious ASL signals” (black arrow heads) and “ASL signal void” (gray arrow heads), likely from eddy current effects, and/or inefficient labeling; while the images acquired with sBIR8-VSS or sinc-VSI pulses were free of such artifacts.

List of tables and figures in Supporting Information

Supporting Information Table 1. The imaging parameters used for all ASL scans in the in vivo experiments. Note that the TR was longer than that in the simulation to accommodate the imaging time.

Supporting Information Table 2. The individual and averaged (mean ± standard deviation) parameters from the correlation and linear regression analysis on ASL signals between different VS labeling schemes and PCASL. There parameters were calculated within the whole brain ROI. One-way ANOVA did not detect any significant difference in the correlation coefficient, the slope and the intercept (P = 0.99, 0.21 and 0.88, respectively) between different VS labeling schemes. The distribution of these parameters across the subjects is shown in **Supporting Information Figure S2**. The subject shown in **Figure 7A** and **Supporting Information Figure S1** was Subject 8.

Supporting Information Figure S1. Scatter plots of the normalized ASL signal in the whole brain ROI, measured with PCASL and different VS labeling schemes from the representative subject (#8) shown in **Figure 7A**.

Supporting Information Figure S2: The boxplots of averaged correlation coefficients, slopes and intercepts across subjects, calculated from the voxelwise correlation and linear regression analysis on the ASL signal within the whole brain ROI for each subject. No statistical significant difference was detected in these parameters between any VS labeling schemes by the ANOVA test.

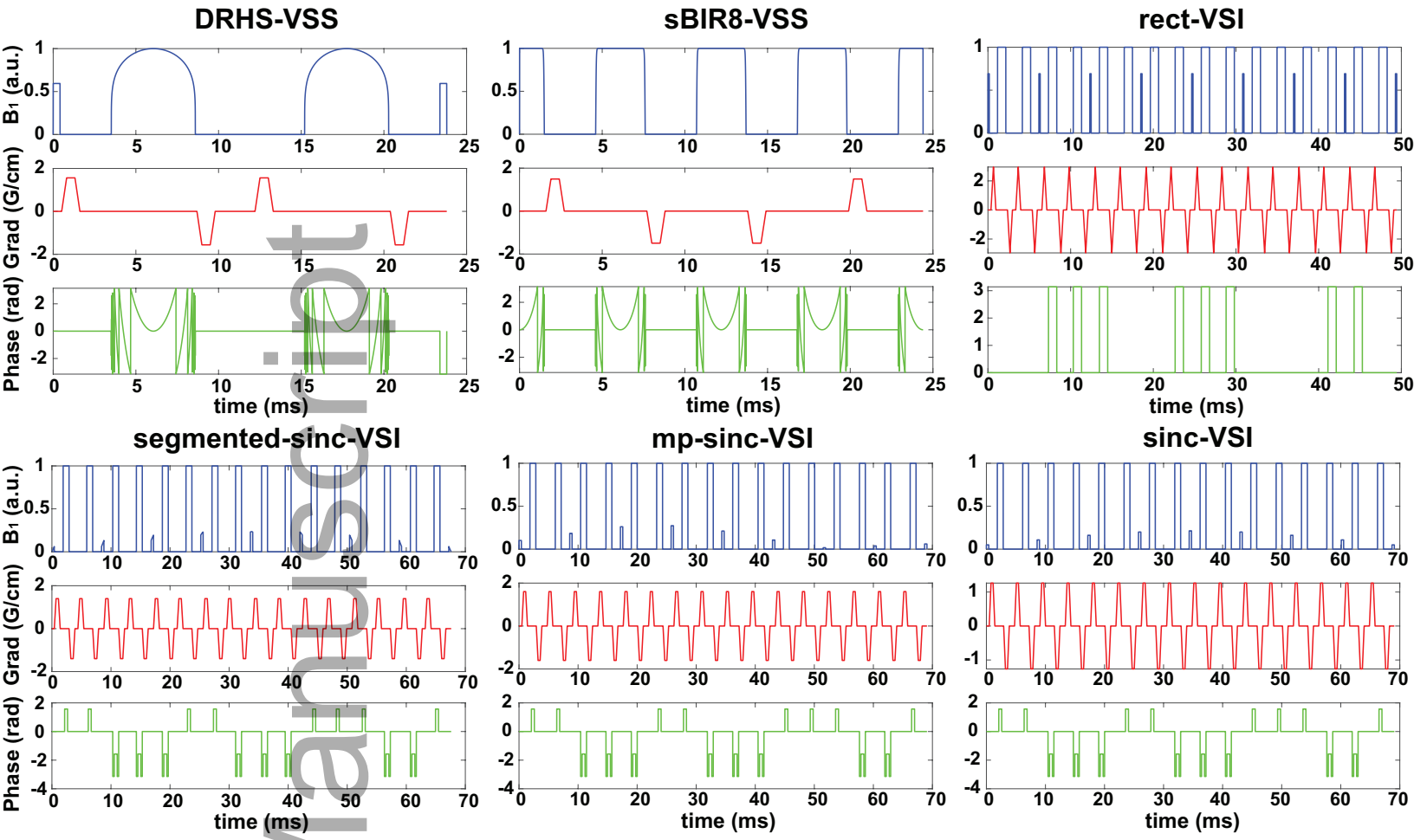

mrm_28572_f1.eps

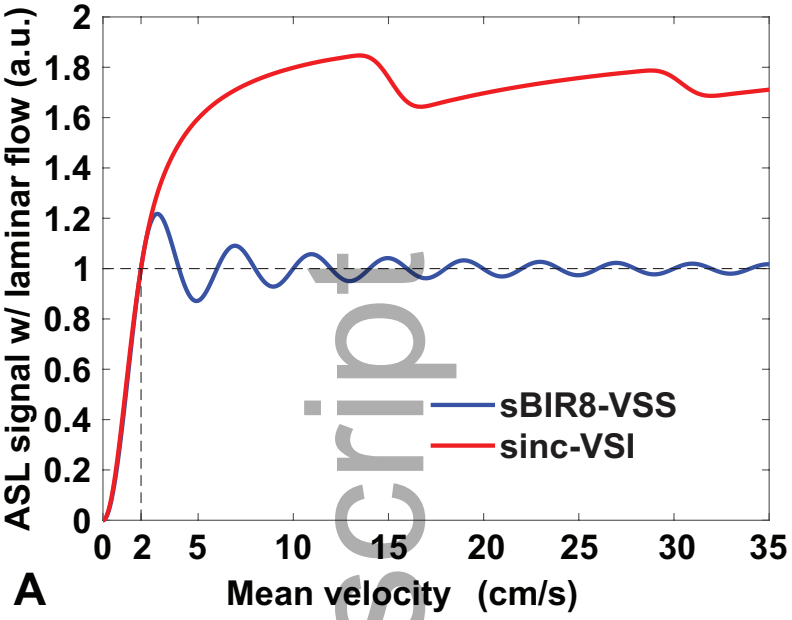

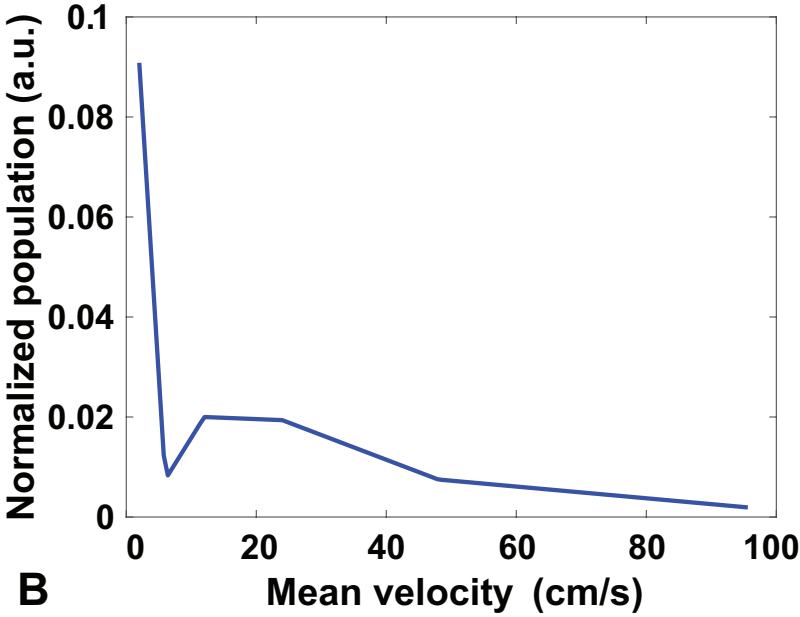

mrm_28572_f2.eps

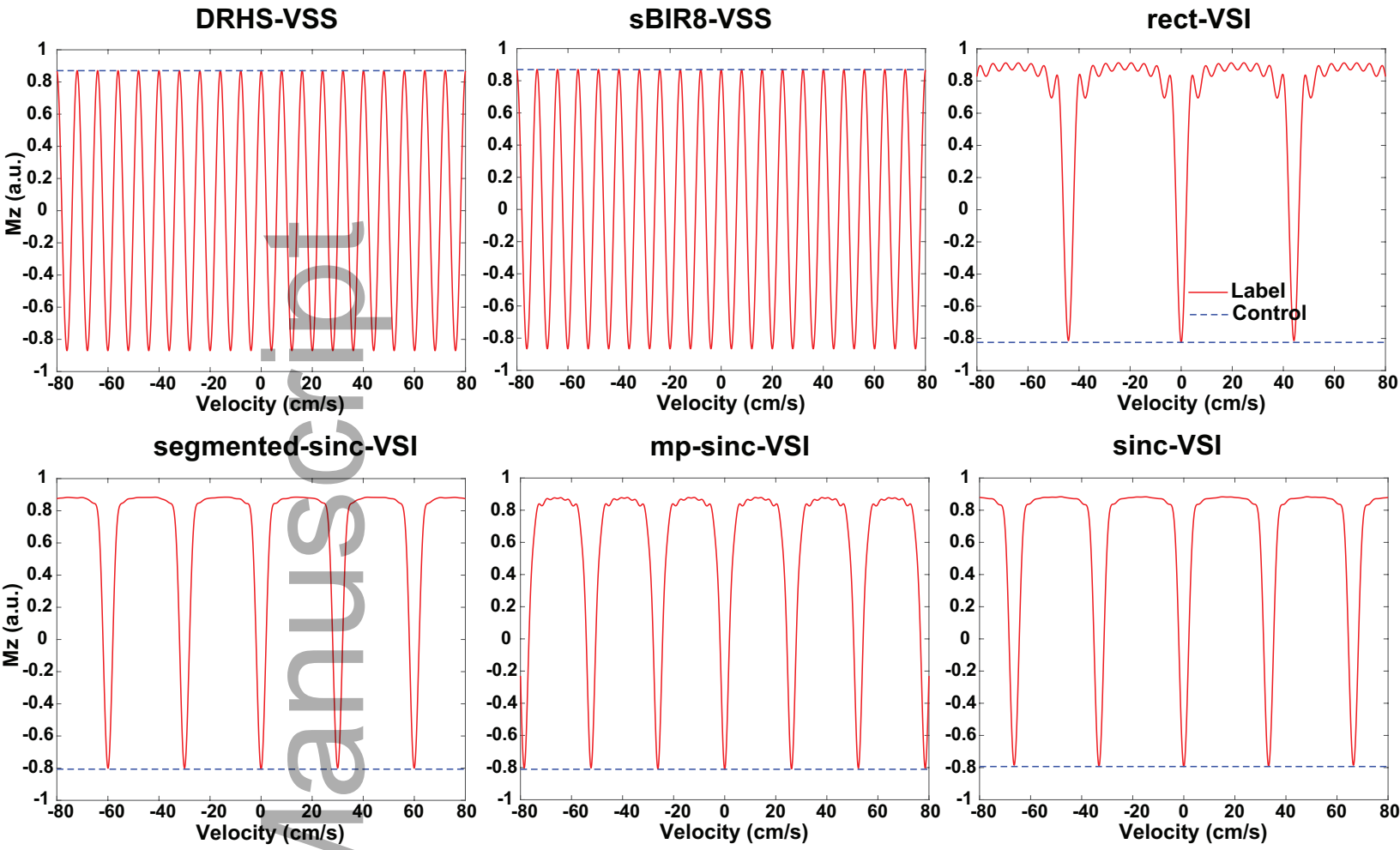

mrm_28572_f3.eps

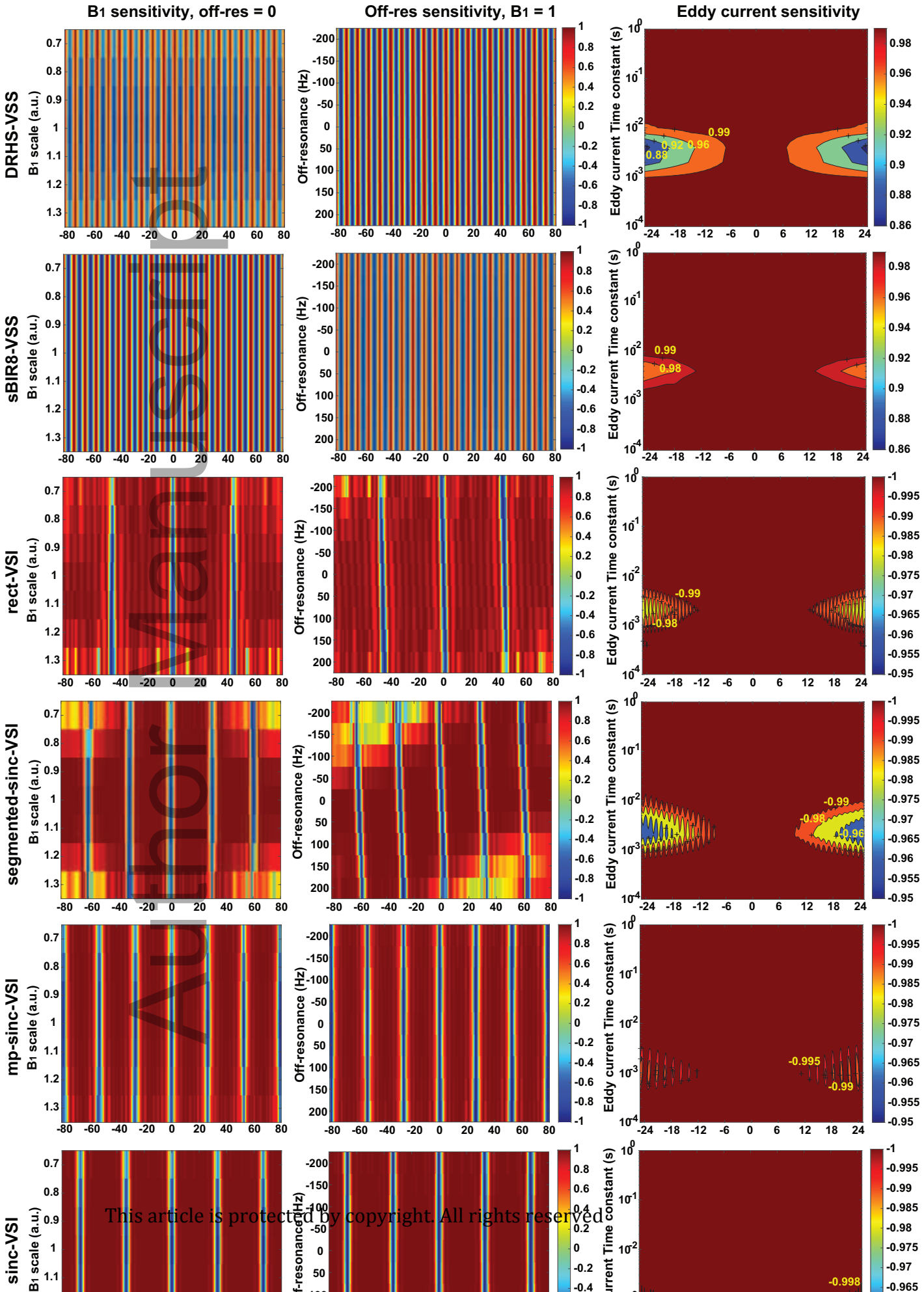

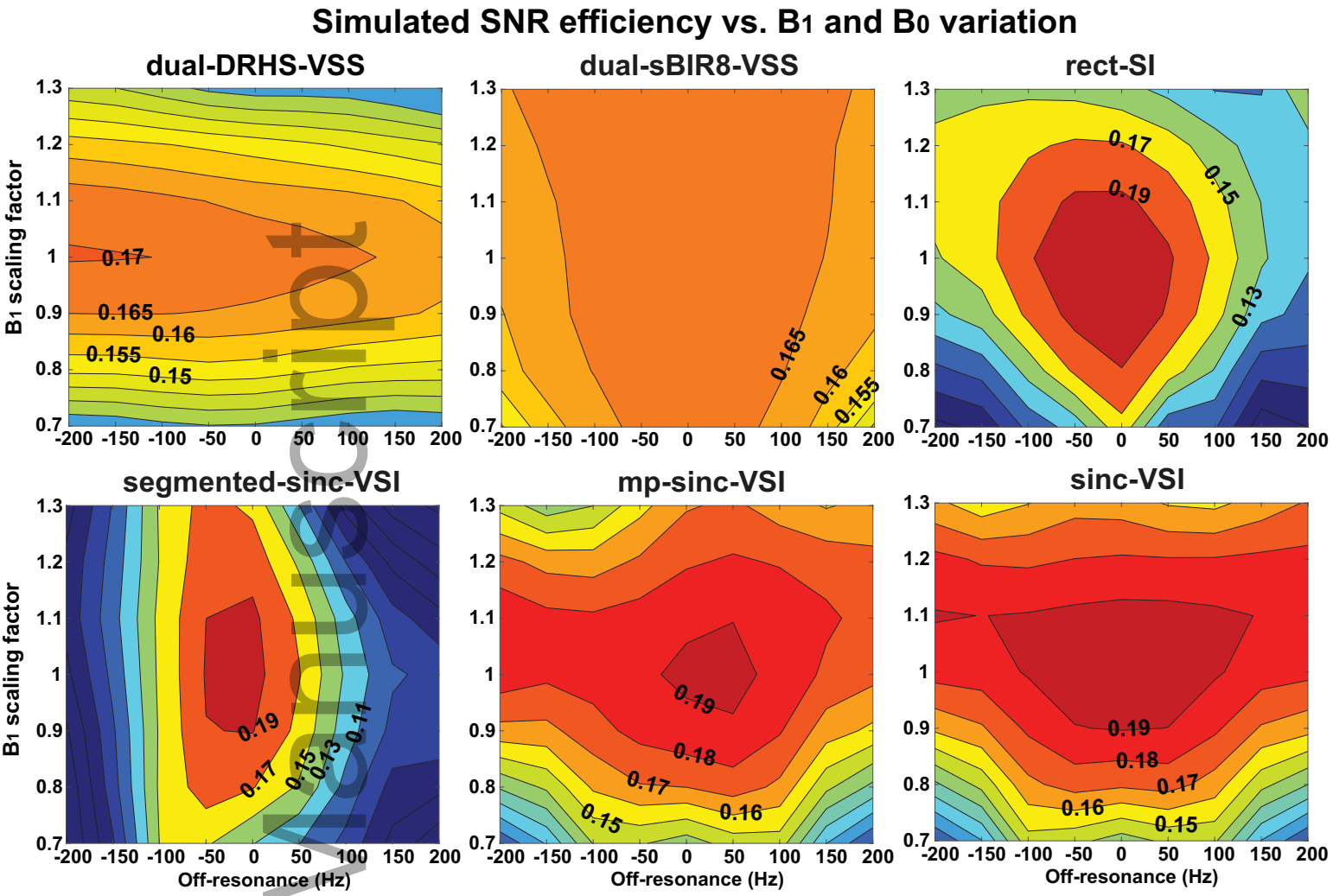

mrm_28572_f5.eps

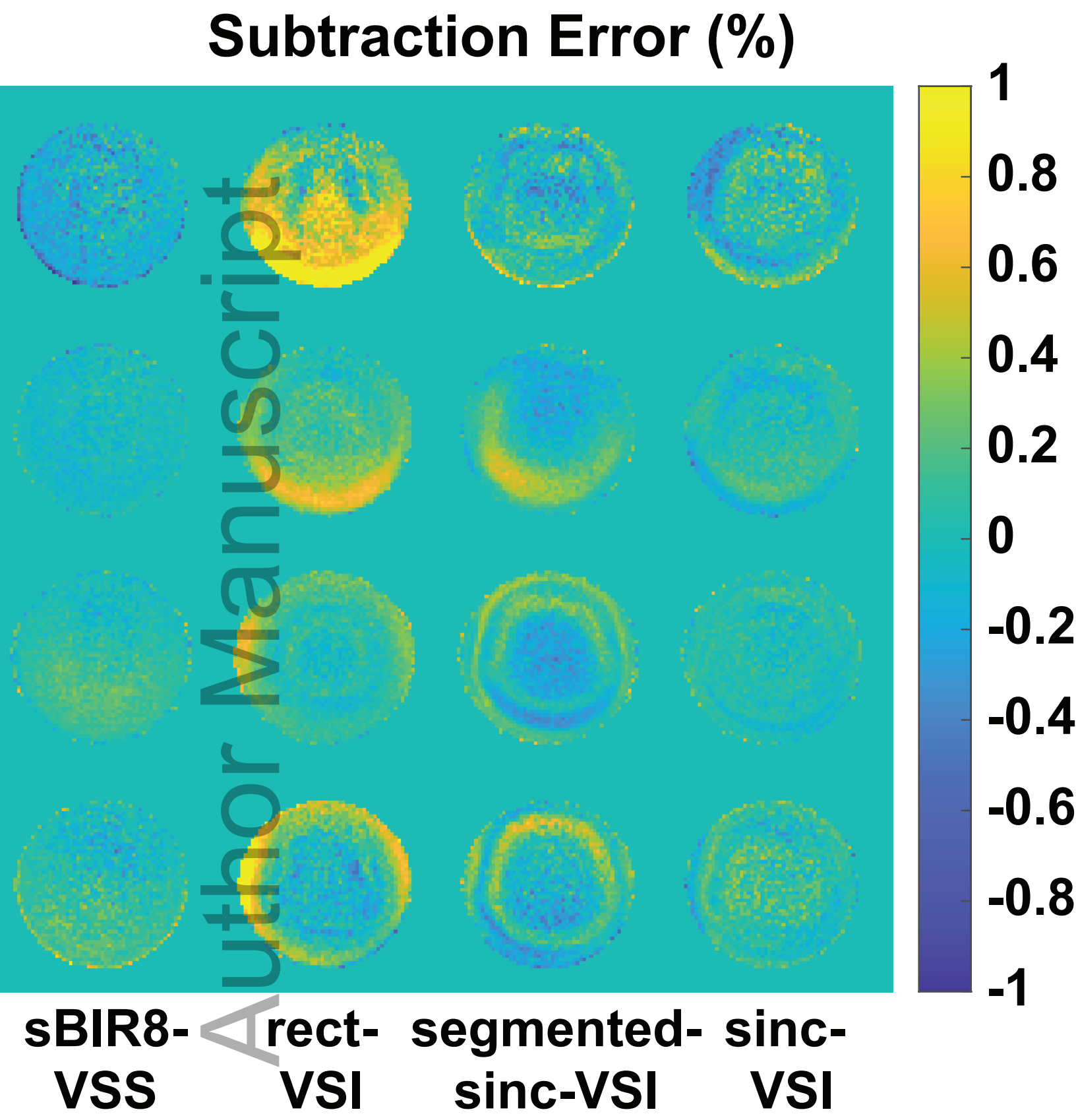

mrm_28572_f6.eps

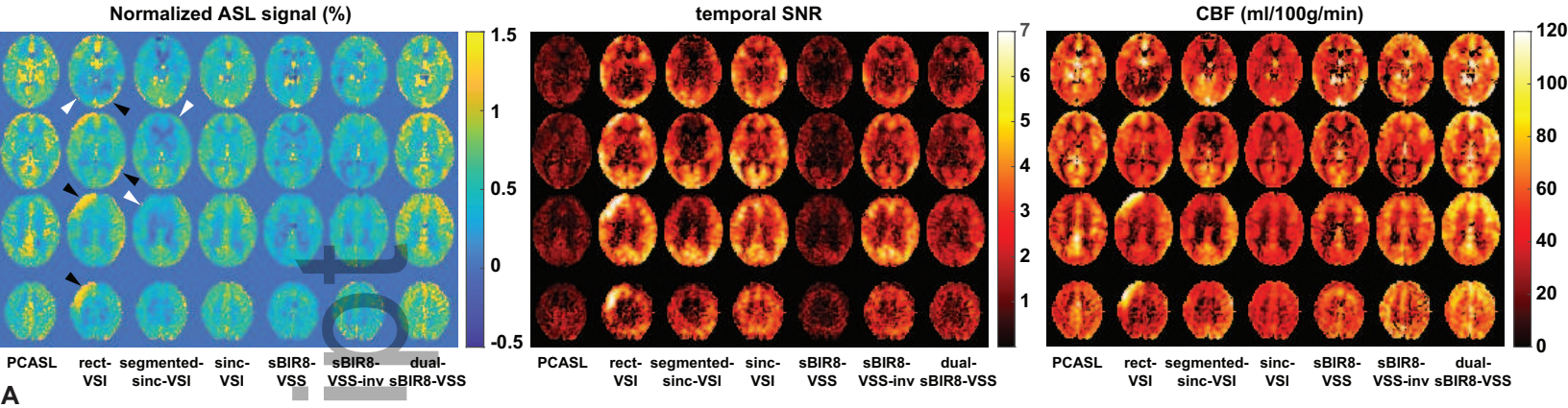

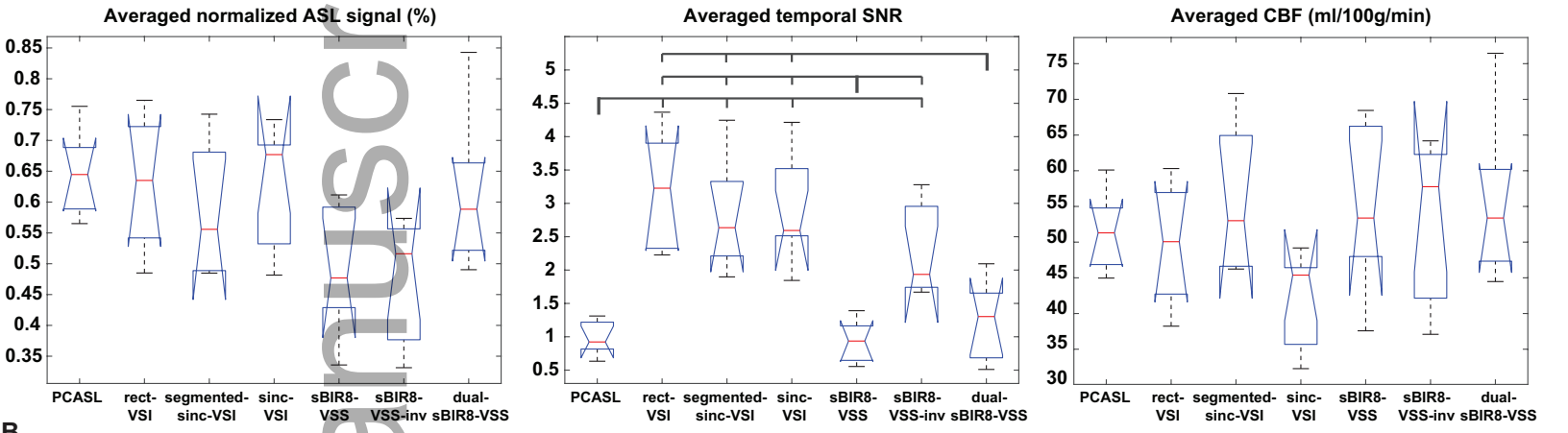

mrm_28572_f7.eps